Available online at www.sciencedirect.com
ScienceDirect
Journal of the European Ceramic Society 26 (2006) 3639–3646
www.elsevier.com/locate/jeurceramsoc

Hydroxyapatite nano-powders produced hydrothermally from nacreous material

A.F. Lemos [a], J.H.G. Rocha [a], S.S.F. Quaresma [a], S. Kannan [a], F.N. Oktar [a,b], S. Agathopoulos [a], J.M.F. Ferreira [a,*]

[a] *Department of Ceramics and Glass Engineering, University of Aveiro, CICECO, 3810-193 Aveiro, Portugal*
[b] *Department of Industrial Engineering, Marmara University, Goztepe Campus, Ziverbey, Kadikoy, 34710 Istanbul, Turkey*

Received 27 October 2005; received in revised form 22 December 2005; accepted 28 December 2005
Available online 10 February 2006

Abstract

Nano-powders of pure AB-type carbonated hydroxyapatite (HA) sized of ~100 nm were successfully produced via hydrothermal transformation (HT) of milled oyster shell powders at 200 °C. Low production cost, worldwide availability and natural-biological origin of raw materials are important features of the investigated process. When fine shell powders were used, the transformation reaction from aragonite to hydroxyapatite was accomplished within about 24 h. Calcite, concentrated at the outer surface of the shells, was less prone to transform into hydroxyapatite under the investigated hydrothermal conditions, even after prolonged reaction time (72 h) or in highly concentrated phosphate solutions.

Keywords: Nacre; Powders-chemical preparation; Microstructure-final; Apatite; Biomedical applications

1. Introduction

Natural species of sea origin, such as corals and nacres, always attract special interest in biomaterials, science and technology. Their bio-mineralization mechanism has been extensively investigated and documented.[1–4] In the particular case of oyster shells, the brick-like structure of nacre (also known as "mother of pearl") is made up of pure aragonite (i.e., a polymorphic phase of $CaCO_3$) crystallized in an organic matrix.[5] The role of protein bio-molecules in the production of aragonite instead of the thermodynamically stable calcite in biological systems has been addressed in several studies.[6–9] Shells usually comprise 96 wt.% mineralized phase, which predominantly consists of $CaCO_3$, and 4 wt.% organic matter; minor amounts of other oxides also exist (0.696% SiO_2, 0.649% MgO, 0.419% Al_2O_3, 0.33% SrO, 0.204% P_2O_5, 0.984% Na_2O, 0.724% SO_3).[10–12]

Nacreous dental implants have been found in Mayan skulls.[13] Many in vitro and in vivo studies[14–23] have suggested nacres as suitable natural materials for dental and bone restorations because they demonstrate ability to initiate and induce mineralized tissue formation by human osteoblasts in vitro and exhibit osteogenic and osteoinductive features by developing bonds with bones.

The present work aims at broadening the prospects of using oyster shells in biomedicine by hydrothermally transforming them into nano-powders of hydroxyapatite (HA, $Ca_{10}(PO_4)_6(OH)_2$). HA is one of the most popular calcium phosphate bioceramics due to its high bioactivity and osseointegration features.[24,25] The natural-biological origin of nacres, containing several trace elements that will remain in the crystalline structure of HA after hydrothermal transformation (HT) making its composition alike human bone, will benefit the overall physiological functioning after implantation.[25,26]

The production of HA from natural aragonite via HT is a known technique since 70s when corals from the Pacific Ocean were transformed into HA-scaffolds that featured great similarities to the mineralized structure of bones.[27,28] The general scheme of the HT reaction is according to the chemical Eq. (1)

$$10CaCO_3 + 6(NH_4)_2HPO_4 + 2H_2O \rightarrow Ca_{10}(PO_4)_6(OH)_2 + 6(NH_4)_2CO_3 + 4H_2CO_3 \quad (1)$$

* Corresponding author. Tel.: +351 234 370242; fax: +351 234 425300.
E-mail address: jmf@cv.ua.pt (J.M.F. Ferreira).

0955-2219/$ – see front matter © 2006 Elsevier Ltd. All rights reserved.
doi:10.1016/j.jeurceramsoc.2005.12.011

Several processing routes, reactors and set-up approaches have been proposed.[29–31] The preservation of corals macrostructure during HT makes them attractive for the production of scaffolds, although their generalized use may meet reservations because corals are species in danger and not available worldwide. This is not the case of common oyster shells.

There are just few reports about the production of HA from nacreous aragonite in the literature. Zaremba et al.[32] have thoroughly investigated the mechanism of HT of aragonite structural units packed in bulk nacre samples, while Ni and Ratner[33] have demonstrated that either aragonite plates or fine powders (<100 μm) of nacreous origin are prone to transform into HA even at room temperature and pH 7.4.

Some additives were shown to play a role during hydrothermal synthesis of different materials. Xu et al.[34] used KH_2PO_4 as mineralizer agent to suppress the production of intermediate non-demanded products during HT of aragonite. Yang et al.[35,36] have used tetraethyl ammonium hydroxide (TENOH) as peptizing agent in the hydrothermal synthesis of nano-powders of TiO_2 and of α-Al_2O_3.

HA nano-powders, currently one of the most demanding challenges for producing new biomaterials, have been tackled only when starting from chemical reagents.[37] To our knowledge, there is no study aiming at producing HA nano-powders from raw materials of natural-biological origin, such as oyster shells. Therefore, the present work aims at preparing inexpensive nano-sized HA particles via HT of oyster shells. The use of nano-powders will enable the high control of chemical and structural features at nano-scale textures of biomaterials. Moreover, nano-powders will enable the production of customized implants using rapid manufacturing techniques like robocasting that involves the extrusion of specially formulated pastes through micron-sized nozzles in combination with CAD/CAM programs.[38]

2. Materials and experimental procedure

Shells from the species *Mytilus galloprovincialis* and *Ostrea edulis* (designated for simplicity purposes hereafter as shells A and shells B, respectively) were collected from Turkish and Portuguese beaches, respectively. Shells A were reduced to a powder simply by hand grinding in an agate mortar. Shells B were crushed and then dry-milled using a planetary mill apparatus for 2 and 6 h and the as-obtained powders were coded as B2 and B6, respectively. The particle size distribution curves of the powders A, B2 and B6 are shown in Fig. 1.

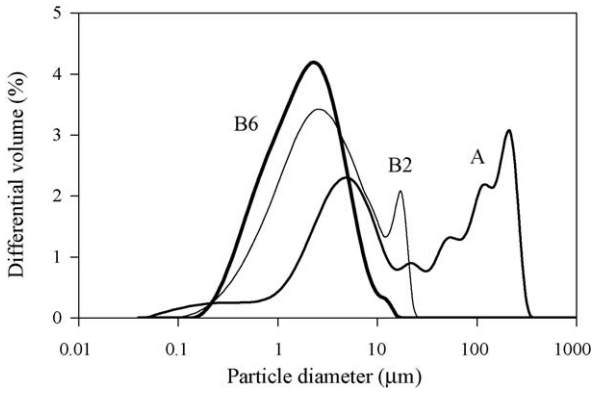

Fig. 1. Particle size distributions of the powders from shells A (A) and shells B after milling for 2 h (B2) and 6 h (B6).

Assuming that the whole matter of the shells consists of $CaCO_3$,[12] mixtures of milled shell powders and an aqueous solution of $(NH_4)_2HPO_4$ were prepared in order to set the molar ratio of Ca/P = 1.67 with the overall concentrations of [Ca] = 2.0 M and [P] = 1.2 M. In one set of experiments using the powder B6, the concentrations of [Ca] and [P] were doubled (i.e., 4.0 and 2.4 M, respectively) and the resulting samples were coded as "B6-x2". The mixtures were sealed in polytetrafluoroethylene (Teflon)-lined stainless steel autoclaves and the hydrothermal transformations took place at 200 °C (heating and cooling rates were 5 K/min) for different times (24, 48, 72 and 92 h) in independent experiments.

With the powder A, two further sets of experiments were also attempted aiming at evaluating the effects of two additives: (a) replacing 50% of $(NH_4)_2HPO_4$ by KH_2PO_4 ($[KH_2PO_4] = 0.6$M); (b) adding 20 wt.% of TENOH with respect to the [Ca]. Table 1 summarizes all the experiments carried out and the corresponding sample codes. The pH of the solution was 9.7 (±0.2) before sealing of the autoclaves and slightly higher after HT (9.8–10.2).

The particle size distributions of the starting powders were measured using light-scattering equipment (Coulter LS 230, UK, Fraunhofer optical model). Differential thermal analysis (DTA/TG, Labsys Setaram TG-DTA/DSC, France, heating rate 5 K/min, in air) was employed to evaluate the thermal behavior of the powdered shells. The crystalline phases of the powders before and after HT were identified by a high resolu-

Table 1
Sample codes and corresponding experimental conditions

Sample code	Powder	$[CaCO_3]$	$[(NH_4)_2HPO_4]$	Additive	HT time (h)
A-92	A	2.0	1.2	–	92
A-92-KH_2PO_4	A	2.0	0.6	0.6 M KH_2PO_4	92
A-92-TENOH	A	2.0	1.2	0.4 M TENOH	92
B2-48	B2	2.0	1.2	–	48
B6-24	B6	2.0	1.2	–	24
B6-48	B6	2.0	1.2	–	48
B6-x2-48	B6	4.0	2.4	–	48
B6-76	B6	2.0	1.2	–	72

tion X-ray diffraction analyzer with monochromatic Cu Kα radiation (λ = 1.5406 Å, XRD, Rigaku Geigerflex D/Mac, C Series, Tokyo, Japan; 2θ step size of 3°/min). Lattice parameters were determined by least square refinements from the well-determined positions of the most intense reflections. The phases were identified by comparing the experimental X-ray diffractograms to standards complied by the Joint Committee on Powder Diffraction Standards (JCPDS) using the cards 09-0432 for HA, 71-2396 for aragonite, and 72-1937 for calcite. Fourier transformed infrared (FT-IR) absorption spectra were recorded between 400 and 4000 cm^{-1} using a Bruker IFS 55 spectrophotometer with a Golden Gate accessory (ATR system of single reflection, Karlsruhe, Germany), using KBr tablets. Microstructure observations were carried out with a scanning electron microscope (SEM, Hitachi S-4100, Japan, 25 kV acceleration voltage) under secondary electron mode.

3. Results and discussion

3.1. Thermal analysis

The results of the thermal analysis (DTA and TG) of the powder from shells A are plotted in Fig. 2 (similar results were obtained from the thermal analysis of shells B). The weight loss (TG curve) due to the organic matter burnt off was ~2–3%. The shells predominantly consist of $CaCO_3$, whose decomposition starts at ~700 °C and peaks at ~900 °C, accounting for a weight loss of about 44% anticipated by Eq. (2):

$$CaCO_3 \rightarrow CaO + CO_2 \quad (2)$$

These results agree fairly well with earlier studies.[5,10–12,32] Two types (1 and 2) of organic matter has been registered in an earlier thorough thermal analysis of nacres.[32] Each type has different rates of weight loss and separate exothermic peaks. In particular, the weight loss due to the organic matter type 1 has been registered between ~70 and 300 °C while the type 2 was burnt out between ~300 and 400 °C. The type 1/type 2 weight ratio was 3.3/0.5. The results of the present study do not distinguish the two types of the organic matter.

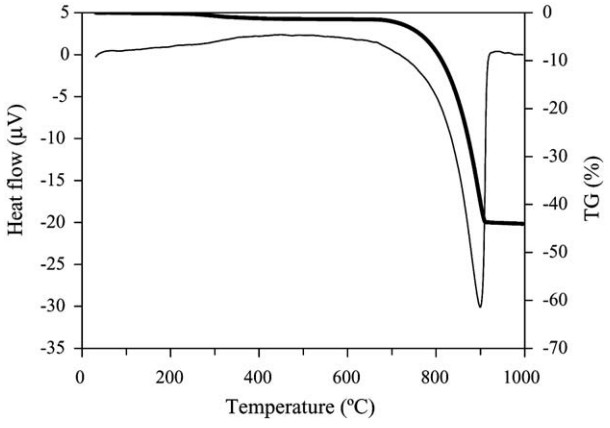

Fig. 2. Thermal analysis (DTA thin line, TG thick line) of powder obtained after milling of shells A (*M. galloprovincialis*).

3.2. Crystalline structure

SEM observations at the inner surface of the shells A revealed a well-stacked lamellar microstructure (Fig. 3). This perfectly oriented microstructure had a tremendous influence in the X-ray diffractograms, as revealed in Fig. 4a. In particular, aragonite was exclusively registered in the spectrum obtained by low incidence X-ray beam to the inner surface of the bulk shell A. Nevertheless, the relationships among the intensities of the peaks significantly differ from standard aragonite (JCPDS card #71-2396), whose X-ray patterns are plotted above this diffractogram. The peak corresponding to the 0 0 2 plane (31.14°), whose intensity is low (4.3%) in standard aragonite, becomes the second dominant in the bulk spectrum. This difference made us to collect powder from the inner surface of the shells by careful scratching of the surface with a lancet and then milled it in an agate mortar. The diffractogram of the collected powder, shown in Fig. 4a, matches fairly well the patterns of standard aragonite. Therefore, the specific layered crystalline microstructure of aragonite, as developed via the bio-mineralization mechanism of nacre in the sea, causes peculiarities in the X-ray diffractogram of bulk nacre. The outer surface of the shells clearly consists of calcite (Fig. 4a) but the relationships among the peak intensities also significantly differed from standard calcite (JCPDS card #72-1937). The influence of sea environment has evidently caused the transformation of the nacreous aragonite into the thermodynamically stable calcite at the outer surface of the shells.

The milled powder of shells A contained both aragonite and calcite (spectrum A of Fig. 4b) that agrees fairly well with the above discussion on the diffractograms of Fig. 4a. There are again slight differences among the relative intensities of the peaks when compared to the patterns of standard aragonite and calcite (Fig. 4b). These differences can be attributed to the wide particle size distribution of the powder A (Fig. 1). The presence of quite big particles of crashed shells in the powder A resulted in a diffractogram that exhibits similarities to that of bulk samples (Fig. 4a).

After 92 h of HT, the powder A was successfully transformed into HA (Fig. 4b). Only weak peaks of aragonite were reg-

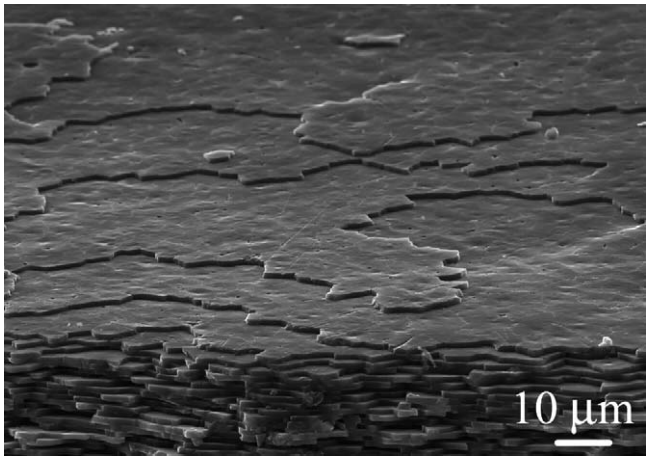

Fig. 3. Lamellar microstructure of the inner (nacreous) surface of shell A (*M. galloprovincialis*).

istered at 2θ 31.14° (plane 0 0 2) and 36.13° (plane 2 0 0). In the presence of TENOH, the peaks of aragonite were more evident, especially at 2θ 31.14° (0 0 2) and 33.15° (0 1 2) as well as at 26.22° (1 1 1), 27.22° (0 2 1), 32.75° (1 2 1), 36.13° (2 0 0 and 1 0 2), 37.91° (1 1 2), 38.63° (0 2 2), 45.86° (2 2 1), and 52.49° (1 1 3). KH_2PO_4 revealed high performance in transforming of aragonite to HA (aragonite peaks were completely vanished from the spectrum) but poor efficiency of the transformation of calcite to HA (Fig. 4b). Together with the main peak at 2θ 29.37° (plane 1 0 4), peaks of calcite were also registered at 23.03° (0 1 2), 35.94° (1 1 0), 39.37° (1 1 3), 43.12° (2 0 2), 47.07° (0 2 4), 47.45° (0 1 8), and 48.45° (1 1 6). Consequently, the most intense XRD peaks of HA along with the weakest presence of other phases were registered in absence of additives (sample A-92).

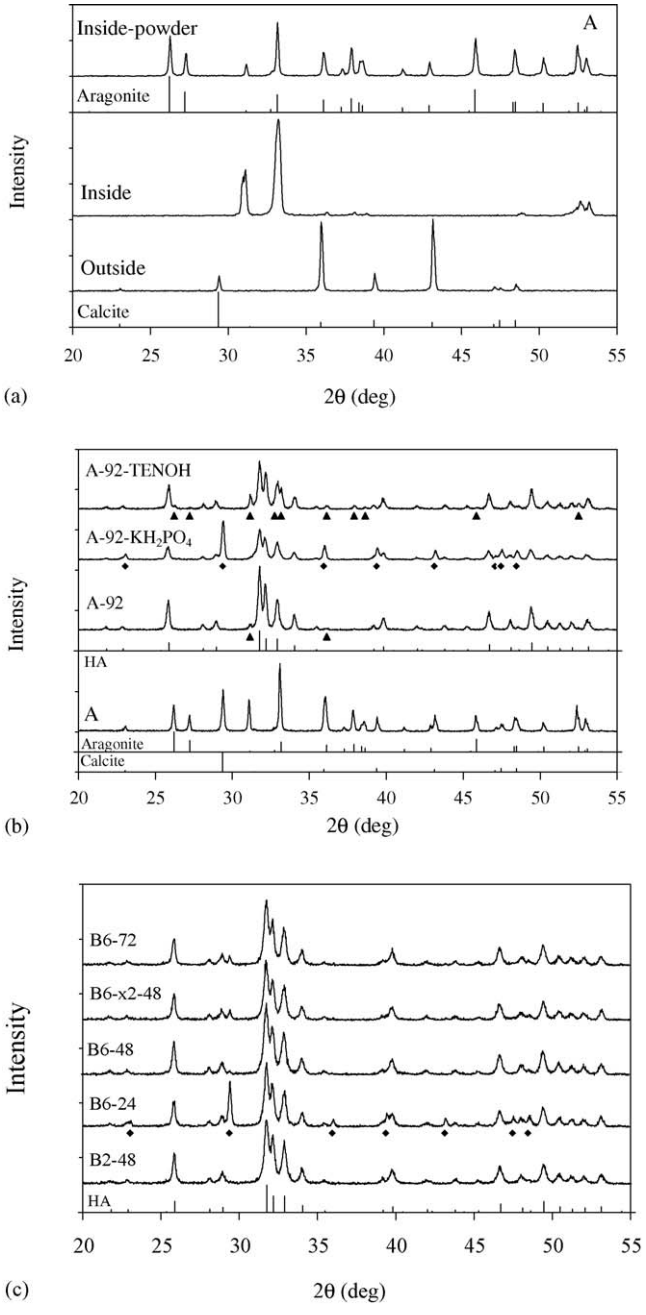

Fig. 4. (a) X-ray diffractograms of the outer (outside) and inner (inside) surfaces of shells A and of the milled powder collected from the inner surface (full scale: 4500 cps). Influence of HT conditions on spectra of powders: (b) shells A (full scale: 16,000 cps); (c) shells B (full scale 12,000 cps). (▲) Aragonite and (♦) calcite. The spectra of the pure phases corresponding to the JCPDS cards #09-0432 (HA), #71-2396 (aragonite) and #72-1937 (calcite) are also plotted. The intensities of the original spectra have not been normalized (see Table 1 for sample codes).

Fig. 3 indicates a very compact aragonite structure with negligible porosity. Consequently, the apparent kinetics of the HT should increase with decreasing the particle size of the starting powders. Hand milling of powder A in a mortar evidently resulted in the wide scattering of particle sizes (Fig. 1). The planetary milled powders from shells B were considerably finer, with the one milled for 6 h (B6) presenting a near Gaussian distribution (Fig. 1).

The fineness of powder B had an obvious positive impact on the kinetics of HT at 200 °C (Fig. 4c). In the case of the powder B2, both aragonite and calcite phases were completely transformed to HA only after 48 h of HT. The results with the powder B6 indicate that the kinetics of HT is fast since highly crystallized HA was obtained after 24 h. There was no evolution of the peaks' intensity between 24 and 72 h.

The crystallographic changes from aragonite and calcite to HA are clearly depicted in the calculated lattice parameters presented in Table 2. The lattice constants of HA for each HT condition tested (calculated from the X-ray spectra of Fig. 4b and c) agree fairly well (±<1%) with the standard values of HA (#09-432). Nevertheless, the different HT conditions tested for powder A considerably affected the crystallite size of HA (Table 2). The larger crystallite size was calculated for the sample A-92-KH_2PO_4. The use of TENOH had an opposite effect reducing the crystallite size near to those calculated for fine powders B, the values of which are relatively insensitive to the HT conditions tested.

From the X-ray diffraction analysis it can be inferred that that aragonite was more susceptible to transform into HA than calcite under the investigated HT conditions. The fineness of the powder

Table 2
Influence of the HT conditions on the lattice parameters and crystallite sizes (D) of hydroxyapaptite (HA, hexagonal-space group, i.e., $a=b$) calculated (±0.0005 Å) from the corresponding X-ray diffractograms (Fig. 4)

Sample code	a-axis (Å)	b-axis (Å)	c-axis (Å)	D (Å)
A-92	9.4182		6.8692	34.53
A-92-KH_2PO_4	9.4118		6.8386	45.25
A-92-TENOH	9.3826		6.8799	29.24
B2-48	9.4366		6.9001	21.41
B6-24	9.4544		6.8755	25.39
B6-48	9.4245		6.8487	26.21
B6-x2-48	9.4381		6.8901	24.64
B6-76	9.4377		6.8702	22.62
HA	9.418		6.884	
Aragonite	4.961	7.967	5.741	
Calcite	4.994		17.081	

The lattice parameters of standard HA (#09-0432), aragonite (#71-2396), and calcite (#72-1937) are also reported.

accelerates the kinetics of HT of aragonite as it can be concluded by comparing Fig. 4c with Fig. 4b. On the other hand, despite the low particle size of the powder B6, the diffraction peaks of calcite were still very intense after 24 h of HT (B6-24), while there were evidences of calcite traces in the other diffractograms of the powder B6 (Fig. 4c). Doubling the concentration of the reagents (B6-2x) did not sufficiently suppress the problem. Consequently, shells richer in aragonite are more suited for HT into HA.

3.3. FT-IR spectroscopy

Fig. 5 presents the FT-IR spectra of all the investigated cases. The spectrum of the starting powder A (Fig. 5a) shows no evidence of the characteristic bands of the functional groups of HA phase. A broad band in the region of 1400–1600 cm^{-1} indicates the presence of the carbonate groups of $CaCO_3$. After HT, the formation of HA is evident according to the characteristic peaks of the PO_4 tetrahedra (ν_3, 1042 and 1088 cm^{-1}; ν_4, 601 and 566 cm^{-1}; ν_1 960 cm^{-1} and ν_2 470 cm^{-1}). The OH group with the characteristic peak at 3570 cm^{-1} (not shown) was doubtlessly obvious in the spectra. The high resolution of the peaks (Fig. 5a) in conjunction with the high intensity of the X-ray peaks (Fig. 4b) indicates the formation of highly crystallized HA-phase.

With regard to carbonates, the analysis of the spectra indicates that the HT process caused the preferential orientation of CO_3 in the apatite lattice (Fig. 5a) as suggested by the vibrational frequencies for CO_3 at 872 cm^{-1} for ν_2 and 1632, 1547, 1458 and 1412 cm^{-1} for ν_3. In general, there are two types of carbonate substitutions on apatites, specifically CO_3 substitution at the OH site (A-type) and at the PO_4 site (B-type), whose presence is reflected in the infrared spectra.[39,40] It has been also found that the occupancy of ν_2 sites occurs competitively between OH^- and CO_3^{2-} groups, whereas the ν_3 sites depend on the competition between PO_4^{3-} ions and CO_3^{2-} ions.[41]

Accordingly, Fig. 5a suggests that the different HT conditions employed in the case of the powder A had different impact on preferred orientation of CO_3^{2-} in the produced HA. In particular, the spectra A-92 and A-92-TENOH feature higher resolution of the bands at 1412, 1458, and 1547 cm^{-1} and a weaker band at 872 cm^{-1} than the spectrum A-92-KH_2PO_4. Hence, it might be qualitatively suggested that the experimental routes of A-92 and A-92-TENOH result in the preferred occupancy of the CO_3^{2-} ions into the PO_4^{3-} sites of apatite while the route A-92-KH_2PO_4 have preferred CO_3^{2-} occupancy at OH^- sites. Consequently, AB mixed type carbonated hydroxyapatite forms after HT process in all cases, where the peculiarities of the preferential orientation of the carbonates are seemingly governed by the specific hydrothermal conditions. Biological apatites, which constitute bone mineral, feature mixed AB type substitutions.[42,43] Therefore, the produced HA powders should perfectly match the implantation aims, since AB-type carbonated apatite spontaneously forms in situ during the HT.

Similar conclusions can be drawn out from the analysis of the FT-IR spectra of the powder B (Fig. 5b), where the characteristic bands of HA phase and the bands due to carbonates have been also clearly registered. The spectrum B6-24 features weak

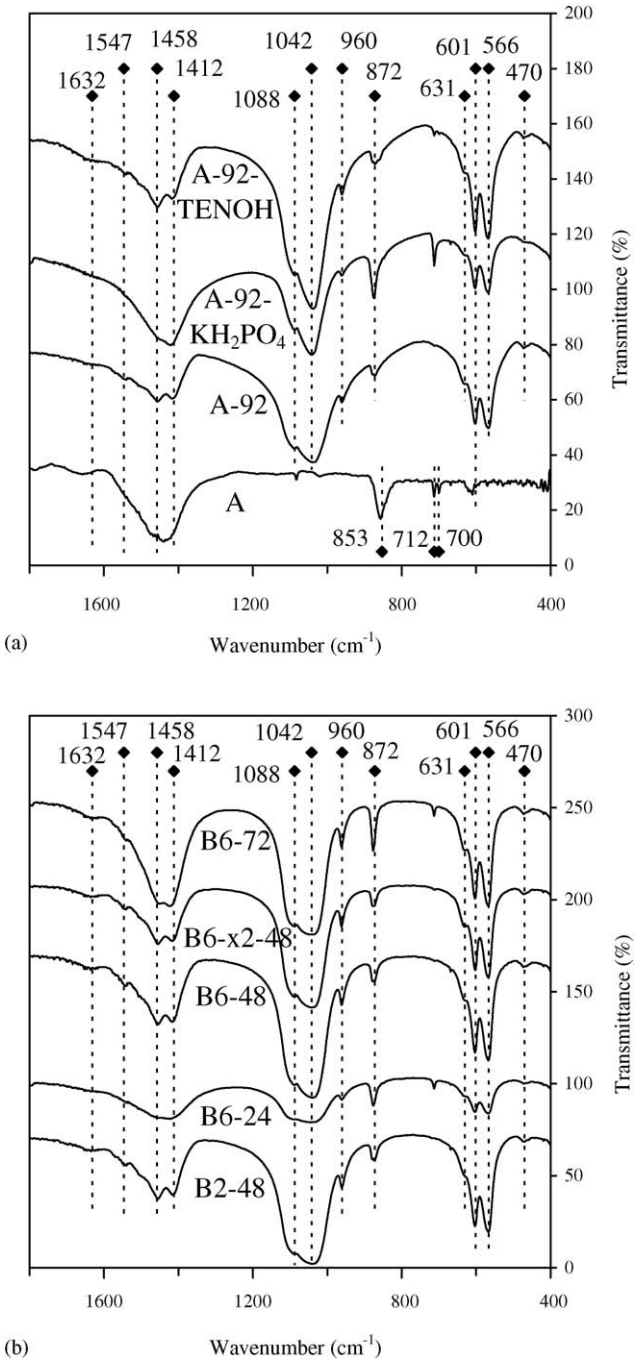

Fig. 5. Influence of hydrothermal conditions on the FT-IR spectra of samples derived from shells A (a) and shells B (b) (see Table 1 for sample codes).

intensity of the bands and poor resolution. According to the corresponding results of the X-ray analysis (B6-24, Fig. 4c), some calcite still remained, as indicated by the high intensity peak at 2θ 29.37°, which likely caused a coupling effect that masked the characteristic bands of HA phase in FT-IR spectra (Fig. 5b).

3.4. Morphology of nano-powders

Fig. 6 shows that nano-sized HA powders were obtained in all the investigated cases. The size of the particles was ~100 nm. There is seemingly no influence of the initial particle size of

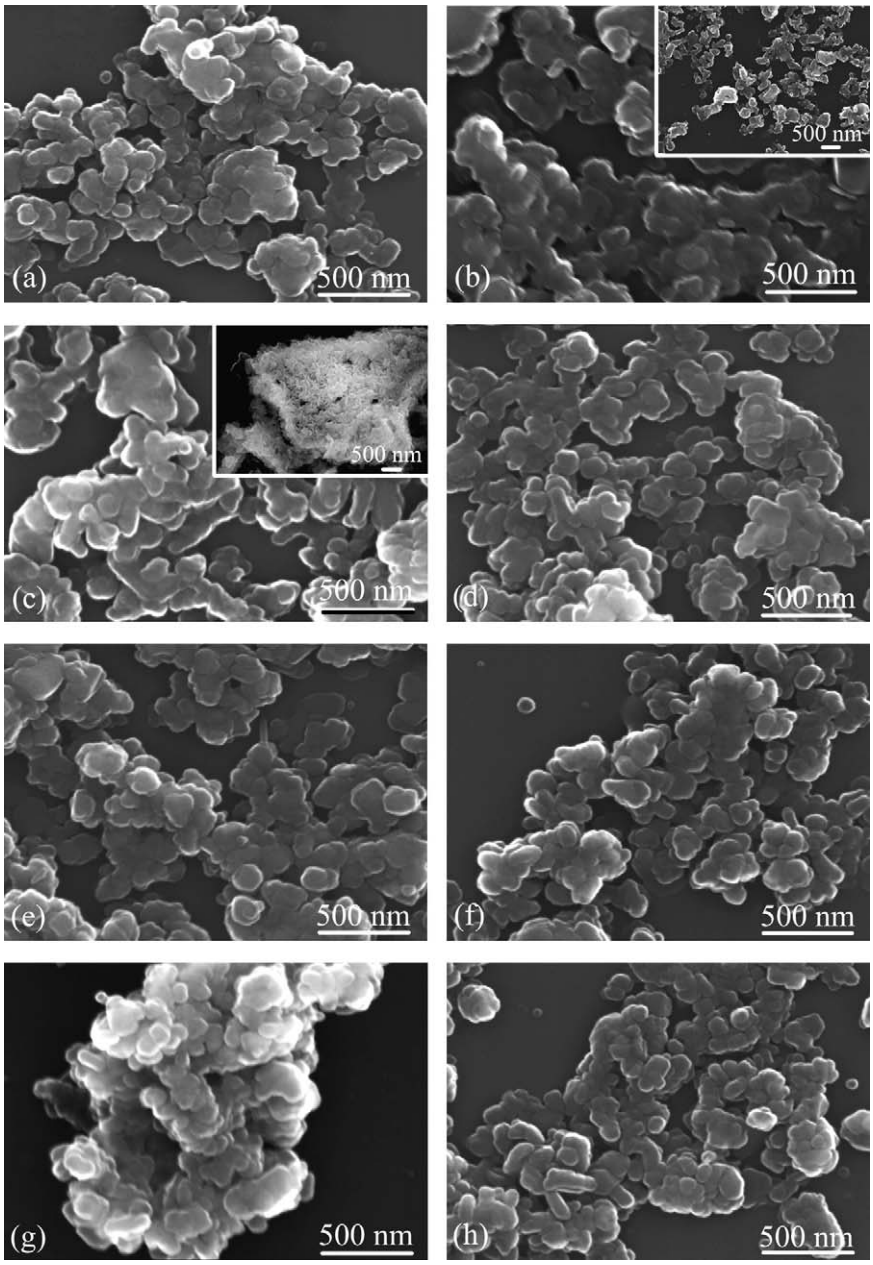

Fig. 6. Influence of hydrothermal conditions on microstructural features of nano-powders (see Table 1 for sample codes): (a) A-92, (b) A-92-KH_2PO_4, (c) A-92-TENOH, (d) B6-24, (e) B6-48, (f) B6-72, (g) B2-48, and (h) B6-x2-48.

the powders (Fig. 1) on the particle size of the resultant powders (Fig. 6a, e and g). Similarly, the HT time (Fig. 6d–f), the additives (Fig. 6a–c) and the concentration of reagents (Fig. 6h) have negligible effect on morphology and particle size of the produced HA powders. In the case of using TENOH, the agglomerates of the particles exhibited the characteristic morphology shown in the inset of Fig. 6c. In all other cases, the particles of the powders were easily dispersed, as shown in the inset of Fig. 6b.

Consequently, the HT of aragonite from shells can be proposed as a method for producing inexpensive HA nano-sized powders at relatively low temperatures (200 °C) and autogenously developed pressures of about 15 atm.[44]

4. Conclusions

Nano-powders of AB-type carbonated hydroxyapatite of ~100 nm of size were produced from powdered oyster shells via HT at 200 °C. The X-ray and FT-IR analyses indicated that the kinetics of the HT into HA is higher in the case of aragonite than calcite. The particle size of the starting powders crucially affected the apparent kinetics of the HT reaction. The use of TENOH favored the reduction of HA crystallite size, increased the efficiency of the transformation of calcite to HA, reduced the performance of aragonite transformation to HA, and resulted in preferred occupancy of the CO_3^{2-} ions into the PO_4^{3-} sites of apatite. The presence of KH_2PO_4 revealed to have an opposite

effect with regards to the crystallite size and the CO_3^{2-} preferential occupancy towards the OH^- sites, and exhibited high efficiency on the transformation of aragonite to HA but poor performance of the transformation of calcite to HA. The worldwide availability and the low cost of oyster shells, along with their biological-natural origin are attractive features conferring to them a high potential for preparing nano-powders of HA for uses in biomedicine.

Acknowledgements

The financial support of CICECO and the Portuguese Foundation for Science and Technology, in the framework of the project POCTI/CTM/60207/2004 and the fellowships of A.F. Lemos (BD/8755/2002), S. Agathopoulos (BDP/1619/2000), and S. Kannan (BPD/18737/2004), are gratefully acknowledged.

References

1. Lowenstam, H. A. and Weiner, S., *On Biomineralization*. Oxford University Press, Oxford, 1989.
2. Wheeler, A. P., George, J. W. and Evans, C. A., Control of $CaCO_3$ nucleation and crystal growth by soluble matrix of oyster shell. *Science*, 1981, **212**, 1397–1398.
3. Manoli, F. and Dalas, E., Calcium carbonate crystallization on xiphoid of the cuttlefish. *J. Cryst. Growth*, 2000, **217**, 422–428.
4. Choi, C. S. and Kim, Y. W., A study of the correlation between organic matrices and nanocomposite materials in oyster shell formation. *Biomaterials*, 2000, **21**, 213–228.
5. Balmain, J., Hannoyer, B. and Lopez, E., Fourier transform infrared spectroscopy (FITR) and X-ray diffraction analyses of mineral and organic matrix during heating of mother of pearl (Nacre) from the shell of the mollusc Pinctada maxima. *J. Biomed. Mater. Res. Part B: Appl. Biomater.*, 1999, **48**, 749–754.
6. Wolf, G. and Guenther, C., Thermophysical investigations of the polymorphous phases of calcium carbonate. *J. Therm. Anal. Calorim*, 2001, **65**, 687–693.
7. Choi, C. S. and Kim, Y. W., A study of the correlation between organic matrices and nanocomposite materials in oyster shell formation. *Biomaterials*, 2000, **21**, 213–222.
8. Smith, B. L., Paloczi, G. T., Hansma, P. K. and Levine, R. P., Discerning nature's mechanism for making complex biocomposite crystals. *J. Cryst. Growth*, 2000, **211**, 116–121.
9. Feng, Q. L., Pu, G., Pei, Y., Cui, F. Z., Li, H. D. and Kim, T. N., Polymorph and morphology of calcium carbonate crystals induced by proteins extracted from mollusk shell. *J. Cryst. Growth*, 2000, **216**, 459–465.
10. Ajakaiye, A., Atteh, J. O. and Leeson, S., Biological availability of calcium in broiler chicks from different calcium sources found in Nigeria. *Animal Feed Sci. Tech.*, 2003, **104**, 209–214.
11. Kwon, H. B., Lee, C. W., Jun, B. S., Yun, J. D., Weon, S. Y. and Koopman, B., Recycling waste oyster shells for eutrophication control resources. *Conser. Recycl.*, 2004, **41**, 75–82.
12. Yoon, G. L., Kim, B. T., Kim, B. O. and Han, S. H., Chemical-mechanical characteristics of crushed oyster-shell. *Waste Manag.*, 2003, **23**, 825–834.
13. Westbroek, P. and Marin, F. A., Marriage of bone and nacre. *Nature*, 1998, **392**, 861.
14. Camprasse, S., Camprasse, G., Pouzol, M. and Lopez, E., Artificial dental root made of natural calcium carbonate (bioracine). *Clin. Mater.*, 1990, **5**, 235–250.
15. Lopez, E., Vidal, B., Berland, S., Camprasse, S., Camprasse, G. and Silve, C., Demonstration of the capacity of nacre to induce bone formation by human osteoblasts maintained in vitro. *Tissue Cell*, 1992, **24**, 667–679.
16. Silve, C., Lopez, E., Vidal, B., Smith, D. C., Camprasse, S., Comprasse, G. *et al.*, Nacre initiates biomineralization by human osteoblasts maintained in vitro. *Calcif. Tissue Int.*, 1992, **51**, 363–369.
17. Lamghari, M., Almeida, M. J., Berland, S., Huet, H., Laurent, A., Milet, C. *et al.*, Stimulation of bone marrow cells and bone formation by nacre: in vivo and in vitro studies. *Bone*, 1999, **25**, 91S–94S.
18. Almeida, M. J., Milet, C., Peduzzi, J., Pereira, L., Haigle, J., Barthelem, M. *et al.*, The effect of water-soluble matrix fraction extracted from the nacre of Pinctada maxima on the alkaline phosphatase activity of cultured fibroblasts. *J. Exp. Zool.*, 2000, **288**, 327–334.
19. Arnaud, E., Pollack, C., Meunier, A., Sedel, L., Damien, C. and Petite, H., Osteogenesis with coral is increased by BMP and BMC in a rat cranioplasty. *Biomaterials*, 1999, **20**, 1909–1918.
20. Atlan, G., Delattre, O., Berland, S., LeFaou, A., Nabias, G., Cot, D. *et al.*, Interface between bone and nacre implants in sheep. *Biomaterials*, 1999, **20**, 1017–1022.
21. Liao, H., Mutvei, H., Sjöström, M., Hammarström, L. and Li, J., Tissue responses to natural aragonite (Margaritifera shell) implants in vivo. *Biomaterials*, 2000, **21**, 457–468.
22. Liao, H., Brandsten, C., Lundmark, C., Wurtz, T. and Li, J., Responses of bone to titania-hydroxyapatite composite and nacreous implants: a preliminary comparison by in situ hybridization. *J. Mat. Sci. Mater. Med.*, 1997, **8**, 823–827.
23. Lamghari, M., Huet, H., Laurent, A., Berland, S. and Lopez, E., A model for evaluating injectable bone replacements in the vertebrae of sheep: radiological and histological study. *Biomaterials*, 1999, **20**, 2107–2114.
24. Dorozhkin, S. V. and Epple, M., Biological and medical significance of calcium phosphates. *Angew. Chem.*, 2002, **41**, 3130–3146.
25. Le Geros, R. Z. and Le Geros, J. P., In *Introduction to Bioceramics*, ed. L. L. Hench and J. Wilson. World Scientific, Singapore, 1993, pp. 139–180.
26. Goller, G., Oktar, F. N., Agathopoulos, S., Tulyaganov, D. U., Ferreira, J. M. F., Kayali, E. S. *et al.*, The influence of sintering temperature on mechanical and microstructural properties of bovine hydroxyapatite. *Key Eng. Mater.*, 2005, **284–286**, 325–328.
27. Roy, D. M. and Linnehan, S. K., Hydroxyapatite formed from coral skeletal carbonate by hydrothermal exchange. *Nature*, 1974, **247**, 220–222.
28. Ben-Nissan, B., Natural bioceramics: from coral to bone and beyond. *Curr. Opin. Sol. State Mater. Sci.*, 2003, **7**, 283–288.
29. Ben-Nissan, B., Milev, A. and Vago, R., Morphology of sol–gel derived nano-coated coralline hydroxyapatite. *Biomaterials*, 2004, **25**, 4971–4975.
30. Jinawath, S., Polchai, D. and Yoshimura, M., Low-temperature hydrothermal transformation of aragonite to hydroxyapatite. *Mater. Sci. Eng. C*, 2002, **22**, 35–39.
31. Ben-Nissan, B., Milev, A., Green, D. D., Hu, J., Conway, R. M., Kannangara, G. S. K. *et al.*, United States Patent No. 20040091547, May 13, 2004.
32. Zaremba, C. M., Morse, D. E., Mann, S., Hansm, P. K. and Stucky, G. D., Aragonite-hydroxyapatite conversion in gastropod (abalone) nacre. *Chem. Mater.*, 1998, **10**, 3813–3824.
33. Ni, M. and Ratner, B. D., Nacre surface transformation to hydroxyapatite in a phosphate buffer solution. *Biomaterials*, 2003, **24**, 4323–4331.
34. Xu, Y., Wang, D., Yang, L. and Tang, H., Hydrothermal conversion of coral into hydroxyapatite. *Mater. Charact.*, 2001, **47**, 83–87.
35. Yang, J. and Ferreira, J. M. F., Hydrothermal synthesis of TiO_2 nanopowders from tetraalkylammonium hydroxide peptized sols. *Mater. Sci. Eng. C*, 2001, **15**, 183–185.
36. Yang, J., Mei, S. and Ferreira, J. M. F., Hydrothermal synthesis of submicrometer alumina from seeded tetraethyl ammonium hydroxide peptized aluminium hydroxide. *J. Am. Ceram. Soc.*, 2003, **86**, 2055–2058.
37. Liou, S. C., Chen, S. Y. and Liu, D. M., Synthesis and characterization of needlelike apatitic nanocomposite with controlled aspect ratios. *Biomaterials*, 2003, **24**, 3981–3988.
38. Jennifer, L., Colloidal processing of ceramics centennial feature aricle. *J. Am. Ceram. Soc.*, 2000, **83**, 2341–2359.
39. Felki, H. E., Savariault, J. M. and Bensalah, A., Structure refinements by the Rietveld method of partially substituted hydroxyapatite:

$Ca_9Na_{0.5}(PO_4)_{4.5}(CO_3)_{1.5}(OH)_2$. *J. Alloy. Compd.*, 1999, **287**, 114–120.

40. Landi, E., Celloti, G., Logroscino, G. and Tampieri, A., Carbonated hydroxyapatite as bone substitute. *J. Eur. Ceram. Soc.*, 2003, **23**, 2931–2937.
41. Rau, J. V., Nunziante Cesaro, S., Ferro, D., Barinov, S. M. and Fadeeva, I. V., FTIR study of carbonate loss from carbonated apatites in the wide temperature range. *J. Biomed. Mater. Res. Part B: Appl. Biomater.*, 2004, **71B**, 441–447.
42. Gibson, I. R. and Bonfield, W., Novel synthesis and characterization of an AB-type carbonate-substituted hydroxyapatite. *J. Biomed. Mater. Res.*, 2002, **59**, 697–708.
43. Elliot, J. C., Holcomb, D. W. and Young, R. A., Infrared determination of the degree of substitution of hydroxyl by carbonate ions in human dental enamel. *Calcif. Tissue Int.*, 1985, **37**, 372–375.
44. Coulson, J. M. and Richardson, J. F., *Tecnologia Quimica*, *Vol I*. Fundação Caloust Gulbenkian, Lisbon, 1974, pp. 512–513.